Human-Robot Control in E-bikes: Modeling and Analysis of a Fatigue-Adaptive Controller

Cason D. Couch
College of Engineering
Georgia Institute of Technology
Atlanta, GA
ccouch31@gatech.edu

Matthew J. McKenna
College of Engineering
Georgia Institute of Technology
Atlanta, GA
mmckenna34@gatech.edu

Ao Li
College of Engineering
Georgia Institute of Technology
Atlanta, GA
aoli@gatech.edu

***Abstract*—Muscular fatigue is a natural byproduct of biking but is only desirable in certain quantities and scenarios. Unwanted muscular fatigue can lead to a less enjoyable bike ride and even result in strain or injury. Therefore, there is a need for fatigue management on E-bikes: to provide the rider with a safer and more enjoyable cycling experience. We sought to develop a fatigue-adaptive controller that provides supplementary power to the bike. As the rider fatigues and produces a decreased power output, the E-Bike's motor compensates by providing greater power to both maintain speed and grant the rider the opportunity to recover from and maintain their fatigue levels. We compare the effects of two controllers: the industry standard power-multiplier controller with our novel fatigue-adaptive controller. We compare both of these controllers by analyzing the E-Bike's electrical power consumption, the cyclist's fatigue, and the speed error across a range of desired biking distances and speeds. The model was simulated with speeds ranging from 5mph to 25mph, and desired distances ranging from 0.1 mile to 1 mile. The results indicate that the fatigue-adaptive controller consumes more electrical power than the power-multiplier controller, but does manage to reduce fatigue compared to the power-multiplier controller at higher speeds while producing similar results at lower speeds.**

I. Introduction

E-bikes are electrically powered bicycles that include a motor and a battery. The motor assists the user in powering the bicycle and enables them to travel greater distances and at higher speeds. E-bikes are often the choice cycling option for the less athletic cyclist or urban commuter. The E-Bike market is rapidly expanding, projected to grow from $43 billion in 2023 to $120 billion by 2030 [1]. The primary motivation for riders switching to E-bikes is the decreased fatigue experienced during riding [2].

During exercise, fatigue can occur for a variety of reasons, most of which encompass metabolite imbalances at the muscle or neurotransmission failures. Acute muscular fatigue is a significant component of any real-world exercise, and at its extremes, it can be an unwanted side effect of biking or increase the risk of accidents or injuries. Fatigue can also be a critical component of exercise or training. Therefore, a solution should be considered, to implement an E-Bike with fatigue-adaptive technology.

The industry standard is a power-multiplier E-Bike, which simply provides electrical power to riding that is proportional to the rider's inputted power [3]. Our goal is to develop a fatigue-adaptive controller to help manage muscular fatigue that takes place during biking. This controller will offer a precisely-fatiguing and more enjoyable riding experience. This controller will also incorporate our model of fatigue to not only compensate for decreased force output from the rider but also provide an increased torque to help the rider recover from their fatigue. The fatigue-adaptive E-Bike will

detect the speed change from the bike and use that to determine the necessary power to compensate for the lost speed. The results from the fatigue-adaptive controller will then be compared to the standard power-multiplier controller. These results will be further analyzed to answer two hypotheses: 1) the fatigue-adaptive controller should consume less power and 2) the fatigue-adaptive controller should leave the rider less fatigued than the power-multiplier controller.

II. Methods

Modeling of this system includes the modeling of an E-Bike, muscle-tendon unit (MTU), multiple human and robot controllers, and muscular fatigue. The various constants involved in this modeling are listed in Appendix A.

A. E-Bike Model

The first step in this study was modeling the E-Bike. A block diagram of the model is shown in Figure 1, which depicts the net free-body diagram in Figure 1(a) and the drivetrain flow in Figure 1(b). The entire model was engineered in MATLAB's Simulink. In the model, the bicycle is propelled forward by an applied force by the wheel on the ground that is produced by the drivetrain. This propelling force is resisted by damping created by aerodynamic drag and rolling resistance, which are both functions of the bicycle's velocity.

Within the drivetrain, the inputs from the human rider and the robot motor are connected to the applied force by the rear wheel on the ground. The human input is represented as the MTU force because the model simplifies the human input to a single MTU. The MTU force applied at the pedal is tangential to the crank rotation. This propels the rotational kinematics of the pedal, but the inefficiencies of the drivetrain cause the pedal kinematics to be continuously slowed by a damping force, which is a function of the angular velocity of the pedal. To further simplify the model, the MTU force is applied only for half of the crank cycle, which is referred to as the power stroke, from the pedal's upright position through the down-stroke to its bottom position. The up-stroke of the cycle

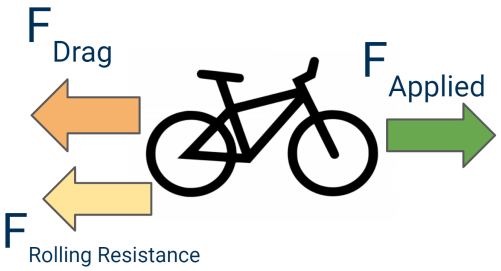

(a)

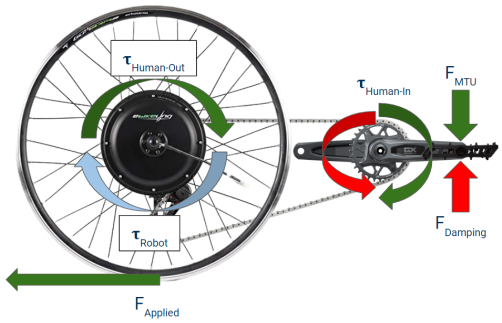

(b)

Figure 1. This free-body diagram depicts the net forces affecting the bicycle's kinematics. (A) The net force on the bicycle is the force applied to the ground by the torque in the rear wheel minus the aerodynamic drag and rolling resistance of the wheels. (B) The drivetrain connects the human rider and robot-controlled motor to the total output force applied by the wheel on the ground. The human torque component, which is resisted by a damping force produced by inefficiencies in the drivetrain, is transformed through several moment arms and gear ratios to produce a final torque on the wheel. The robot torque is applied directly to the wheel, so the sum of human and robot torque produces the force applied on the ground by the wheel.

serves to restore the MTU to its resting state before performing another power stroke. The model does not include a second leg, so the human force is applied in pulses with a duty cycle of approximately 50%. Note that the damping force is not constrained to only the power stroke, and instead continuously acts to slow the rotation of the pedal.

Further illustrating the modeling of the drivetrain, the product of net force on the pedal during the power stroke and the radius of the crank produces a torque at the crank. This input torque is transformed by a fixed gear ratio according to Equation 1, where τ_{out} is torque out, τ_{in} is torque in, n_{out} is teeth on

out-gear, and n_{in} is teeth on in-gear.

$$\tau_{out} = \tau_{in} \frac{n_{out}}{n_{in}} \tag{1}$$

The output torque depicts the human component of torque on the rear wheel. The E-Bike's robot motor uses direct-drive torque assistance, which means that the electrically powered torque is applied directly to the rear wheel. The sum of the human and robot torques produces a force on the ground by the rear wheel that acts to propel the bike forward, denoted as the applied force.

For simplicity, the human input was modeled as a singular plantar-flexion MTU rather than multiple musculoskeletal joints and systems. This MTU is modeled in accordance with the methodology described in Exploiting Elasticity, depicted in Figure 2 [4]. This entails modeling the muscle as a contractile element in parallel with an elastic component. The muscle is connected in series with an elastic element representing the tendon. This MTU produces a force that is transformed by the effective moment arm produced by the ankle's lever mechanics, which is determined by the lever length and fulcrum positioning. The MTU force is a function of many internal components but is primarily controlled by the activation of the muscle. This activation is driven by the stimulation signal produced by the central nervous system and sent to the muscle. The model enables the human rider to modulate the amplitude of the stimulation signal, but it is confined to the power stroke, which means there is never any stimulation during the recovery stroke.

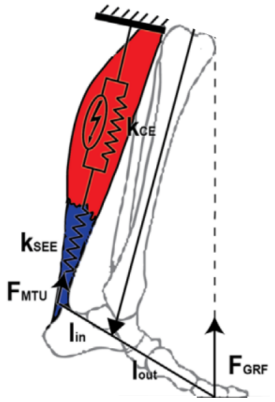

Figure 2. The MTU model as described in Exploiting Elasticity [4]. The model describes a contractile element with a parallel elastic component, which represents the muscle, connected in series with an elastic element, which represents the tendon. The MTU force is transformed by an effective moment arm based on the fulcrum location and level lengths on the ankle bones.

B. Fatigue

Another physiological concept that was introduced and modeled was acute, muscular fatigue. Our fatigue model conglomerates central and distal fatigue, with the resulting effect being a decreased maximum exertable muscular force. A more complex model from Ma et al. was originally used [5], but was eventually simplified by the team to include a binary fatigue and recovery state. The developed equation is shown in Equation 2, where F_{cem} is the current exertable muscle force, $K_{recovery}$ is the recovery coefficient, $K_{fatigue}$ is the fatigue coefficient, $a(t)$ is muscular activation, and $u(t)$ is neural stimulation.

$$\frac{\mathrm{d}F_{cem}}{\mathrm{d}t} = \begin{cases} K_{recovery} \cdot (1 - a(t)) & u(t) = 0 \\ -K_{fatigue} \cdot a(t) & u(t) > 0 \end{cases} \tag{2}$$

The F_{cem} described in the equation functions as the maximum force the muscle can produce at a given time due to its history of fatigue and recovery within the simulation. It is confined within the range of $(0, F_{max}]$. During periods with no stimulation, the muscle will undergo recovery as a function of the lingering muscular activation, while during stimulation, the muscular activation will contribute to fatigue of the muscle.

With the model for F_{cem} established, the metric for measuring fatigue was developed as a function of F_{cem} and F_{max}, such that it described the portion of true maximum force no longer usable due to fatigue. This notion is represented in Equation 3.

$$\text{Fatigue} = 1 - \frac{F_{cem}}{F_{max}} \tag{3}$$

This measure is used to gauge the exhaustion of a rider and will be a useful metric in measuring the success of our new controller in mitigating fatigue.

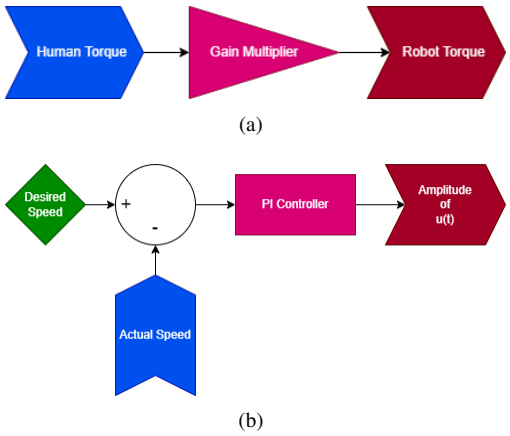

Figure 3. (A) The control model for the robot motor is a multiplied value of the measured human torque contribution. (B) The human torque model uses a PI controller with speed error as an input and stimulation amplitude as an output.

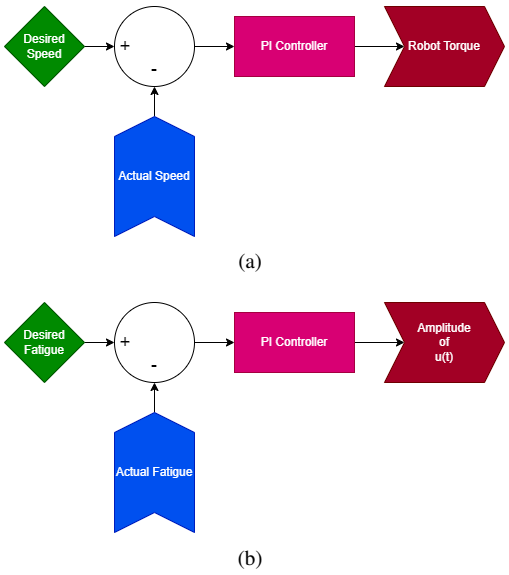

Figure 4. (A) The control model for the robot motor is a PI controller referencing the bike's speed error and outputting torque. (B) The human control model is a PI controller referencing fatigue error and outputting stimulation amplitude.

C. Controller Models

Both the human rider and the robot motor are modeled with controllers that dictate their torque outputs. The control laws are reflective of the selected control mode: either Power-Multiplier Control (PMC) or Fatigue-Adaptive Control (FAC).

1) Power-Multiplier Control: In PMC mode, the robot serves to multiply the power contributions (i.e. torque) of the human rider. This is reflective of the industry standard for E-Bike control [3]. In this model, the human must then modulate their own torque contributions by modulating stimulation amplitude in order to maintain the desired riding speed. The two controller block diagrams are depicted in Figure 3. This model implies a torque sensor capable of real-time sensing of human torque contributions and a bike speedometer. Additionally, the control model checks a threshold speed error, above which the human will cease sending stimulation signals.

2) Fatigue-Adaptive Control: This controller is of our own design and seeks to maintain speed using the robot motor while the human maintains a desired fatigue level. For the robot, this involves a simple PI controller that produces an output torque as a function of the bike's speed error. The human instead uses a PI controller to produce different levels of stimulation as a function of fatigue error. This model implies a bike speedometer and that the human has an accurate awareness of their current level of fatigue. Additionally, the control model checks a threshold speed error, above which the human will cease sending stimulation signals. The block diagrams for these controllers are depicted in Figure 4.

D. Experiment

To evaluate the effectiveness of our FAC E-Bike compared to the standard PMC E-Bike, we conducted an experiment in which the rider rode for a set distance aiming to maintain a desired speed. The tested speeds were from 5-25 mph with increments of 5 mph. These speeds were each tested for distances of 0.1-1 miles with increments of 0.1 miles. During these tests, a desired fatigue value was set to 20%. For each of these conditions, both control modes were tested. During each test, we collected the torque contributions of both the human and the robot, fatigue levels, bike speed, and distance covered over time.

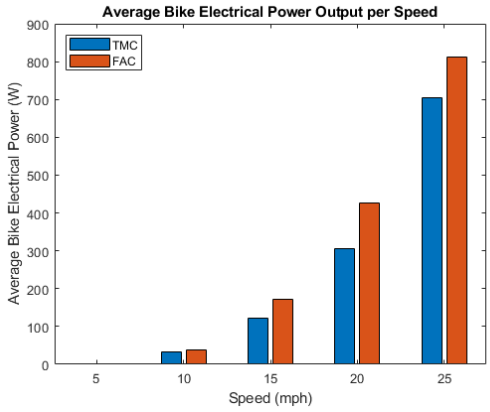

Figure 5. Average Bike Electrical Power Output per Speed for the FAC (Red) and PMC (BLUE) controllers. The FAC generally consumes more power at each speed compared to the PMC.

Table I
AVERAGE SPEED ERROR (RMSE)

	Speed (mph)				
	5	10	15	20	25
PMC	0.681	0.640	1.517	2.776	4.642
FAC	0.549	0.852	1.572	2.442	3.451

III. RESULTS

A. Electrical Power Output

The electrical power consumption of the E-Bike motor differed between the FAC and PMC as shown in Figure 5. After averaging for distance traveled, the PMC had a lower power consumption in 4 of the 5 speeds and consumed an average of 56.364 W less than the FAC.

B. Fatigue

Meanwhile, the Average Fatigue Percent of the rider varied with velocity and distance. Between the 5-20mph cases, the PMC had an average of 0.0456 and a standard deviation of 0.0049, while the FAC had an average of 0.0521 and a standard deviation of 0.0051 (reported as decimals). These low fatigues and similarities between both controllers deviated in the 25mph case as the FAC had 0.1799 less fatigue percent than the PMC controller (0.1336 vs 0.3135).

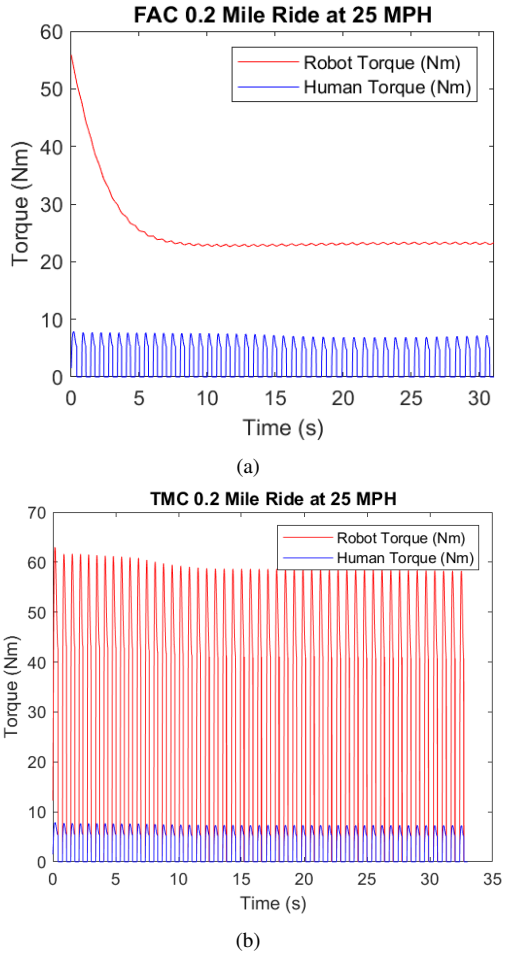

Figure 6. Robot and Human Torque vs Time for 0.2 Miles at 25 MPH. (A) The FAC Torque vs Time exhibits how the fatigue-adaptive controller adjusts the Robot (E-Bike) Torque to the person's fatigue by applying a continuous Torque. (B) The PMC Torque vs Time shows how the assistive Robotic E-Bike torque is a direct multiple of the human's torque resulting in large discontinuous spikes

IV. DISCUSSION

The FAC did not result in a decrease in electric power consumption of the E-Bike motor compared to the PMC, therefore the first hypothesis is rejected. Meanwhile, the FAC only showed significant improvements in fatigue reduction in 1 of the 5 tested speeds, so the results regarding the second hypothesis are inconclusive.

Specifically, as seen in Figure 5, the difference between the larger FAC and lower PMC electric power consumption is significant. This difference in power is the result of higher average torques in the FAC compared to the PMC. This is because the PMC strictly multiplies the torque of the human, so when the human's torque is zero during the upstroke, which in this instance is 0.375 s of the 0.75 s pedaling period, the robot torque is also zero. This is in contrast to the continuous torque the FAC applies over time. So even though the PMC typically applies a higher max torque than the FAC, its average power is less due to its cyclically zero torque output.

Meanwhile, the fatigue (as defined by Equation 3) differs based on distance and speed as shown in Figure 7. At the 5-20 mph speeds, both the FAC and PMC had consistently low average fatigues with little deviation. This is due to high MTU F_{cem} values since the rider's performance doesn't decrease significantly at these lower speeds. The fatigue trends greatly differ for the 25 MPH speed. Here the fatigue percent increases for both controllers, with the FAC greatly outperforming the PMC. The improved performance of the FAC is due to its accounting for the difference between the desired and actual fatigues of the rider. While the performance of the FAC at 25mph is a significant improvement, this result alone is not enough to validate the original hypothesis. Seeing the beginning of this trend occurring at 25 mph, future research would likely benefit from testing at higher desired speeds to better understand this trend.

Lastly, to evaluate the extent to which the cyclist and E-Bike system successfully maintained the desired speed, the Root Mean Squared Error (RMSE) was averaged and organized in Table I. The FAC and PMC deviate more as the speed increases because the bike takes longer to reach the larger, desired speed. The FAC has lower RMSE values than the PMC in 3 of the 5 cases and performs significantly better at 25 mph. This is likely due to the continuous speed control of the FAC compared to the PMC. Overall, these RMSE values are still significant, so further tuning of controllers representing the human and E-Bike should be pursued to reduce these speed errors.

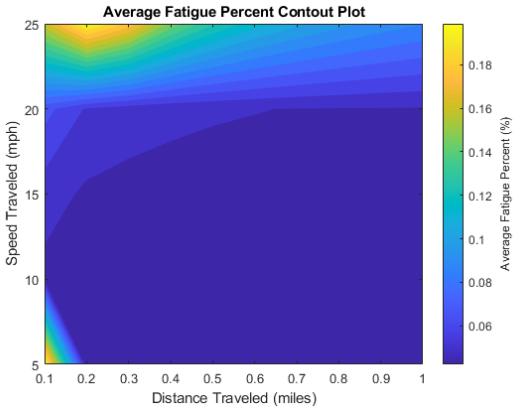

(a)

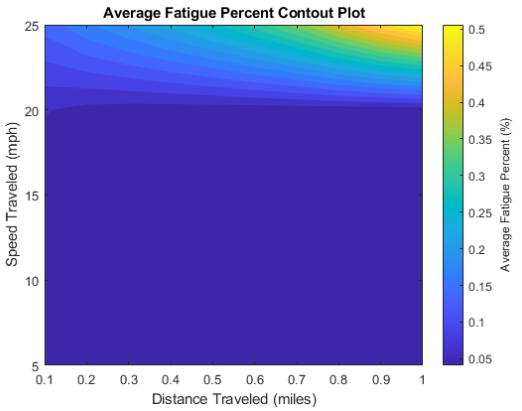

(b)

Figure 7. Fatigue plots of Distance (.1mile-1mile) vs Speed (5-25MPH) vs Fatigue (percentage in decimal form). (A) Shows the FAC Fatigue is low for low speeds but increases at 25 mph speeds. A similar trend can be seen for the PMC Fatigue plot (B). Overall the FAC results in lower Fatigue at 25 mph but similar results elsewhere when compared to the PMC.

Future work could include testing of different desired fatigue conditions since all testing was only conducted with a constant desired fatigue of 20%. More insight could be gained from varying the rider's desired fatigue based on their cycling objective (recreation, exercise, commuting) or as a function of time, helping to personalize the riding experience for each user. Additionally, increasing the desired speed or distance could offer a fruitful

analysis. Since most U.S. state laws regarding E-bikes limit the legal maximum speed to 28 mph (such as Georgia House Bill 454 [6]), it may be useful to look at increased maximum distance rather than just increased speeds. Longer cycling distances could result in substantially different fatigues for the FAC compared to PMC and support its effectiveness. Lastly, future work should model a second MTU to more accurately simulate the dynamics of both of the cyclist's legs and should consider expanding the human input to involve more complex musculoskeletal dynamics than standalone MTUs.

V. Conclusion

Inconsistent with the proposed hypothesis, the FAC failed to consume less power than the PMC. The FAC only managed to reduce fatigue at high speeds but performed similarly to the PMC at lower speeds. The fatigue-adaptive controller is not currently recommended as a replacement for the standard power-multiplier controller, but further work could be done to improve its capabilities and further analyze its performance benefits.

Acknowledgements

Thank you Dr. Sawicki and Dr. Young for teaching the awesome course: Biomechatronics of Wearable Robotics.

References

[1] "Electric bike market size," *Fortune Business Insights*, vol. 1, p. 1, 2023.

[2] "E-bike market size share, trend, and growth report 2030," *Market Research Report*, 2021.

[3] K. Schleinitz, T. Petzoldt, L. Franke-Bartholdt, J. Krems, and T. Gehlert, "The german naturalistic cycling study–comparing cycling speed of riders of different e-bikes and conventional bicycles," *Safety science*, vol. 92, pp. 290–297, 2017.

[4] B. D. Robertson and G. S. Sawicki, "Exploiting elasticity: modeling the influence of neural control on mechanics and energetics of ankle muscle–tendons during human hopping," *Journal of theoretical biology*, vol. 353, pp. 121–132, 2014.

[5] L. Ma, D. Chablat, F. Bennis, and W. Zhang, "A new simple dynamic muscle fatigue model and its validation," *International journal of industrial ergonomics*, vol. 39, no. 1, pp. 211–220, 2009.

[6] "Hb 454 motor vehicles; operation of motorized mobility devices." [Online]. Available: https://www.legis.ga.gov/legislation/55353

[7] R. Legg, "Fluid flow:general principles," 2017.

[8] P. N. Doval, "Aerodynamic analysis and drag coefficient evaluation of time-trial bicycle riders," 2012.

[9] P. Debraux, W. Bertucci, A. Manolova, S. Rogier, and A. Lodini, "New method to estimate the cycling frontal area," *International journal of sports medicine*, pp. 266–272, 2009.

[10] W. J. v. Steyn and J. Warnich, "Comparison of tyre rolling resistance for different mountain bike tyre diameters and surface conditions," *South African Journal for Research in Sport, Physical Education and Recreation*, vol. 36, no. 2, pp. 179–193, 2014.

[11] S. C. Walpole, D. Prieto-Merino, P. Edwards, J. Cleland, G. Stevens, and I. Roberts, "The weight of nations: an estimation of adult human biomass," *BMC public health*, vol. 12, no. 1, pp. 1–6, 2012.

[12] P. Minarik, "How much do road bikes cost and weigh? (data from 647 bikes)," 2023.

APPENDIX A

Table II
LIST OF CONSTANTS

Name	**Symbol**	**Value**	**Reference**
Air Density	ρ_{air}	$0.01\frac{\text{m}}{\text{s}^2}$	[7]
Drag Coefficient	C_{drag}	0.68	[8]
Effective Area of Bike and Rider	$A_{effective}$	0.5m^2	[9]
Rolling Resistance Coefficient	$\mu_{rolling}$	0.002	[10]
Damping Coefficient (Drivetrain Inefficiency)	$C_{damping}$	30	
Human Rider Mass	m_{human}	62kg	[11]
Bicycle Mass	m_{bike}	8.32kg	[12]
Pedal Mass	m_{pedal}	5kg	
Crank Radius	r_{crank}	0.17m	
Teeth on Out-Gear	n_{out}	39	
Teeth on In-Gear	n_{in}	53	
Wheel Radius	r_{wheel}	0.311m	
Fatigue Constant	$K_{fatigue}$	500	
Recovery Constant	$K_{recovery}$	250	
Maximum Muscular Force	F_{max}	6000N	[4]
Maximum Muscular Velocity	v_{max}	$-0.45\frac{\text{m}}{\text{s}}$	[4]
Length of Maximal Contraction Force	l_{m_0}	0.055m	[4]
Slack Tendon Length	$l_{t_{slack}}$	0.237m	[4]
Activation Time Constant	τ_{act}	0.033s	[4]
Deactivation Time Constant	τ_{deact}	0.091s	[4]
Effective Moment Arm	$EMA(\frac{l_{in}}{l_{out}})$	0.33	[4]
Desired Fatigue	$1-\frac{F_{cem}}{F_{max}}$	0.2	